ELSEVIER

Colloids and Surfaces
A: Physicochemical and Engineering Aspects 122 (1997) 135–149

COLLOIDS AND SURFACES A

A novel contact angle measurement technique by analysis of capillary rise profile around a cylinder (ACRPAC)

Yongan Gu, Dongqing Li *, P. Cheng

Department of Mechanical Engineering, University of Alberta, Edmonton, Alberta, T6G 2G8, Canada

Received 9 May 1996; accepted 1 September 1996

Abstract

A new experimental technique and its computational scheme to determine the contact angles of capillary rise profiles around a cylinder are presented. In the experiment, a carefully coated conic glass cylinder was inserted vertically and slowly into a tested liquid. Then the precise image of the partial capillary rise profile of the liquid around the conic cylinder was acquired and digitized by applying computer image processing and analysis techniques. From the digitized profiles of the liquid–vapour interface and the conic cylinder, the local inclination angle β and the local radius R_c, of the conic cylinder at the three-phase contact circle were calculated directly. Furthermore, an objective function was constructed, which expresses the discrepancy between the physically observed capillary rise profile and the theoretically predicted curve, i.e. the curve representing a solution of the Laplace equation of capillarity. The contact angle of the capillary rise profile on the conic cylinder was used as an adjustable parameter in optimizing the objective function and determined once the minimum objective function had been achieved. The accuracy of the measured contact angles is approximately 0.1°. In addition to the local gravity, the densities of the liquid and vapour phases and the liquid–vapour surface tension, the input requirement is the digital information of the partial capillary rise profile which is provided by a specially designed computer image analysis program. This method was tested by measuring contact angles of four n-alkane liquids around cylindrical glass fibres coated with FC725. The measured contact angles are in very good agreement with those determined by the Wilhelmy plate technique. Finally, the present technique was also applied to study the dependence of contact angles on the geometry of the conic cylinder, i.e. on $\cos \beta/R_c$. Contact angles of the four n-alkane liquids on a conic glass cylinder coated with FC725 were measured at different positions along the cylinder. The results were interpreted in terms of the line tension effect. The calculated line tensions were positive and of the order of 1 $\mu J\ m^{-1}$, which is consistent with the published data for similar solid–liquid systems obtained by using the sessile drop method. In particular, the contact angle without line tension effect θ_∞ for a given solid–liquid system can be measured directly by this method. The validity of the derived contact angle θ_∞ and line tension σ was also confirmed by means of the axisymmetric drop shape analysis (ADSA) technique. This novel technique is particularly suitable to the study of the wetting and spreading phenomena of a liquid on fibres, as most fibre surfaces are rough and their shapes may deviate considerably from those of right circular cylinders. A general user-oriented computer program to implement the technique was developed.

Keywords: Capillary rise; Contact angle; Fibre; Line tension

* Corresponding author.

PII S0927-7757(96)03853-8

1. Introduction

The contact angle is an important quantity in many areas of applied science and engineering. Physically, the contact angle of a liquid on a solid provides a basis for the study of the interaction between the two phases. Changes in the angle reflect changes in the net interactions across the interface and changes in the compositions and environmental conditions of bulk phases forming the interface. It is well known that studies of wettability, adhesion, adsorption and flotation require knowledge of the contact angle [1–3]. Measurement of the contact angle can also be used to determine solid surface tensions [4] and to study thin-liquid-film phenomena [5,6] and line tension effects [7–12].

There have been many experimental techniques available for contact angle measurements. Reviews of these methods can be found elsewhere [1,3,13–18]. Of all the methods employed to measure contact angles, direct measurement from sessile drops is probably the most popular approach. The measurement is performed by using a telescope equipped with a goniometer eyepiece. The contact angle is determined by aligning a tangent with the drop profile at the point of the three-phase contact circle on the solid surface. In addition to its experimental simplicity, the sessile drop method requires only small quantities of liquid and solid surface. However, there are some difficulties remaining with this simple method whenever high accuracy and consistency are needed. A precision of $\pm 2^\circ$ is usually claimed. Alignment of the tangent is subjective and depends on the experience of the operator. In recent years, a sophisticated sessile drop method, the axisymmetric drop shape analysis (ADSA) technique [19–21], has been developed to determine the contact angles and the interfacial tensions simultaneously. The accuracy of the ADSA technique is about 0.1° for contact angle measurements. In the sessile drop method the contact angle is dependent on the drop size; this is often referred to as the line tension effect. The contact angles can increase by as much as $3–10^\circ$ as the base radius of the sessile drop on the solid substrate changes from, say, 1 to 5 mm [8–10]. Therefore, the sessile drop method cannot directly measure the contact angle θ_∞, which is the contact angle of an infinitely large drop with no line tension effect. A detailed discussion of the line tension effect and its determination from measured contact angles has been given previously [22] and will be summarized later.

The Wilhelmy plate technique [1,15,23,24] is an alternative method in which the contact angle is determined by measuring the height of capillary rise at a vertical flat plate. In this method, the contact angle is determined from the height of capillary rise at a vertical plate, according to

$$\sin \theta_\infty = 1 - \frac{\Delta\rho\, g h^2}{2\gamma_{lv}} \tag{1}$$

where $\Delta\rho = \rho_l - \rho_v$ is the density difference between the liquid phase and the vapour phase, g is the acceleration due to gravity, γ_{lv} is the surface tension of the liquid–vapour interface, h is the capillary rise height and θ_∞ is the contact angle of the capillary rise profile on the vertical plate. The best precision of contact angles obtained by this technique is about $\pm 0.1^\circ$. The Wilhelmy plate method can avoid the line tension effect on contact angles, as the three-phase contact line in this case is a straight line.

The sessile drop method, the Wilhelmy plate method and most other contact angle measurement techniques require a flat solid surface, and hence cannot be used to measure contact angles on curved surfaces, such as a cylindrical fibre surface. However, the determination of the contact angles or wettability on fibre is of practical importance in the composite materials, textile and cosmetic industries. The Wilhelmy–Gravitational method is probably the only existing technique suitable for this kind of measurement. In this method, a fibre hanging on an electrobalance is partially immersed in a test liquid. The contact angle is determined by measuring the force F required to balance the fibre according to the following equation [15]:

$$F = P\gamma_{lv} \cos\theta - V\Delta\rho g \tag{2}$$

where P is perimeter of the fibre, and V is the liquid volume displaced by the fibre, or the volume of the fibre immersed in the liquid. The major limitation of this method is that accurate values

of P, γ_{lv}, V and $\Delta\rho$ have to be known. For non-porous fibres with a smooth surface, such as a glass fibre, P and V can be measured and remain constant during the experiment. Thus the reproducibility of contact angle results may be satisfactory in this case. However, fibres usually do not have constant diameters, i.e. their perimeters change along their axial direction. Furthermore, for a porous fibre, the perimeter and the volume of the fibre will change during the measurement because of the penetration of liquid into the fibre which causes a change in the fibre's shape (swollen). Therefore, contact angle results are generally difficult to reproduce by using the Wilhelmy–Gravitational method.

Recently, drop methods have also been used to determine the contact angle of a liquid on a fibre surface. In the method developed by Yamaki and Katayama [25] and Carroll [26], the contact angle is determined indirectly by measuring the shape of a liquid droplet and using an analytical solution of a differential equation governing the shape of the droplet on a fibre in the absence of gravity. Unfortunately, such measurements of contact angles were unable to provide an accuracy better than about 5°. This was partly due to the fact that there is a great deal of error involved in obtaining the contact angle by reading from a plot of the reduced droplet length against the reduced maximum droplet thickness, as reported by other researchers [27,28]. The visual problems presented by the dimensions and shape of fine fibres, the irregular surface, and the anisotropic characteristics of most fibres make it very difficult to obtain reproducible results. The scatter in the data was also attributed to the surface heterogeneity and variable diameter of the fibre. Later, Wagner [27] proposed two simple extensions of the above method and claimed that better results of the apparent contact angles of a liquid drop formed on a thin cylindrical monofilament might be obtained. More recently, Ogawa and Ikeda [29] have improved Carroll's method and Wagner's interpolation technique. Furthermore, Kumar and Hartland [30,31] gave the numerical solution of the differential equations governing the shape of a drop on a vertical fibre in the presence of gravity, and presented a technique for measuring the so-called upper and lower contact angles. Good agreement was found between their measured contact angles and their theoretical predictions. In general, these experimental techniques are exclusively limited to first measuring the dimensions and shape of a liquid droplet on a fibre surface and then relating them to the contact angle either analytically or numerically. The results of these techniques are usually not accurate and depend on the droplet size and many other factors.

In the present paper, a new experimental technique for determining contact angles by the analysis of a liquid–vapour interface around a cylinder is presented. This method, analysis of capillary rise profile around a cylinder, will be referred to as simply ACRPAC hereafter. In this method, the precise image of a partial capillary rise profile of the liquid around a conical or constant-diameter cylinder was acquired and digitized by applying computer image processing and analysis techniques. The contact angle of the capillary rise profile on the cylinder was then determined by numerically minimizing the deviation between the physically observed (the digitized) capillary rise profile and the theoretically predicted curve. The latter is the curve representing a solution of the Laplace equation of capillarity. The accuracy of the measured contact angles is approximately 0.1°. Besides the local gravity, the densities of the liquid and vapour phases and the liquid–vapour surface tension, the only input datum required is the digitized partial capillary rise profile. The contact angles determined by the ACRPAC method are insensitive to reasonable uncertainties involved in these input data. As will be seen in later sections, the ACRPAC method was first used to measure the contact angles of four n-alkane liquids around cylindrical glass fibres coated with FC725. The results obtained are in good agreement with those obtained using the Wilhelmy plate method. This new method was then applied to study the dependence of contact angles on the geometry of the conical glass cylinders, which was interpreted as the line tension effect. In particular, the contact angle without the drop size effect θ_∞ can be measured directly by the present method. Using a computer image analysis technique, the ARCPAC method is fully automatic, objective and accurate.

It will be particularly suitable for the precise measurement of the phenomenological contact angles of a liquid on irregularly shaped fibres. A general user-oriented computer program package for implementing this technique is now available.

In the following sections, we first present the numerical solution of the differential equations governing the shape of the capillary rise profile around a conical cylinder in the presence of gravity. The objective function is then defined as a measure of the deviation of the calculated Laplacian curve from the measured capillary rise profile. This function is the average of the "normal" distances between the measured points and the calculated curve. The optimization of the objective function is achieved by using the contact angle as one of the adjustable parameters. A computational scheme for determining the contact angle is developed. Next, the detailed experimental set-up and procedure, digital image acquisition and digitization processes are described. Finally, the measured contact angles on constant-diameter and conical cylinders as well as their application to the determination of the line tension of four *n*-alkane liquids on the FC725 solid surface are given and discussed. Comparisons are made of the experimental data obtained in this work and the data obtained with both the sessile drop method using the ADSA technique and the Wilhelmy plate technique.

2. Theory

When a conical cylinder is inserted vertically into a pool of liquid, the liquid will climb up the cylinder above the undisturbed surface of the liquid. As illustrated in Fig. 1, the liquid–vapour interface will form a contact angle with the surface of the conical cylinder. For a moderately curved liquid–vapour interface, the pressure difference across the curved interface is described by the classical Laplace equation of capillarity:

$$\Delta P = P_l - P_v = \gamma_{lv}\left(\frac{1}{R_1} + \frac{1}{R_2}\right) \tag{3}$$

where ΔP is the pressure difference across the liquid–vapour interface, P_l and P_v are the pressures on the liquid side and on the vapour side of the interface, respectively, γ_{lv} is the surface tension of the liquid–vapour interface, and R_1 and R_2 are the principal radii of curvature of the interface. In the absence of external forces other than gravity, the pressure difference is a linear function of the elevation. For an arbitrary point $P(x,y)$ on the liquid–vapour interface, the pressures in Eq. (3) can be expressed as

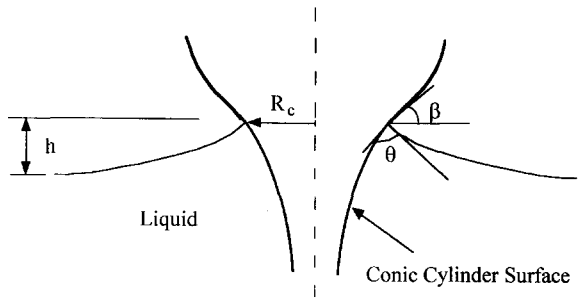

Fig. 1. Schematic diagram of the capillary rise profile around a conical cylinder.

$$P_l = P_{l0} - \rho_l g y \tag{4}$$

and

$$P_v = P_{v0} - \rho_v g y \tag{5}$$

where ρ_l and ρ_v are the densities of the liquid and vapour phases, respectively, y is the local capillary rise height of point $P(x,y)$ on the interface above the horizontal undisturbed surface of the liquid, P_{l0} and P_{v0} are the reference pressures of the liquid and the vapour phases, respectively, chosen at the vicinity of the undisturbed surface of the liquid. If the ratio of the radius of the conical cylinder to the radius of the pool is sufficiently small, the difference between the two reference pressures ΔP_0 will be zero by applying Eq. (3) at $y=0$, i.e. on the undisturbed flat liquid–vapour interface, and noting that $R_1^0 = R_2^0 = \infty$,

$$\Delta P_0 = P_{l0} - P_{v0} = 0 \tag{6}$$

where R_1^0 and R_2^0 are the principal radii of curvature of the undisturbed liquid–vapour interface far from the cylinder axis. Substituting Eqs. (4)–(6)

into Eq. (3) and rearranging gives

$$\gamma_{lv}\left(\frac{1}{R_1}+\frac{1}{R_2}\right)=-\Delta\rho g y \tag{7}$$

where $\Delta\rho=\rho_l-\rho_v$ is the density difference between the liquid phase and the vapour phase. For the system illustrated in Fig. 1, the xy coordinate system was chosen as follows: the y axis is the axis of the conical cylinder, and the x axis is along the horizontal undisturbed liquid–vapour interface and normal to the y axis. The Laplace equation of capillarity (Eq. (7) can be rewritten as

$$\frac{\dfrac{d^2y}{dx^2}}{\left[1+\left(\dfrac{dy}{dx}\right)^2\right]^{3/2}}+\frac{\dfrac{dy}{dx}}{x\left[1+\left(\dfrac{dy}{dx}\right)^2\right]^{1/2}}=\frac{\Delta\rho g y}{\gamma_{lv}} \tag{8}$$

Eq. (8) is a second-order ordinary differential equation that requires two boundary conditions. The convenient choice of the boundary conditions are the capillary rise height and the contact angle on the solid conical cylinder surface. At the three-phase contact circle on the conical cylinder, the capillary rise height h, the tangential angle ϕ and the contact angle θ of the liquid–vapour interface constitute the related boundary conditions:

$$y|_{x=R_c}=h \tag{9}$$

$$\frac{dy}{dx}|_{x=R_c}=-\tan\phi=-\tan(180^\circ-\beta-\theta)=\tan(\beta+\theta) \tag{10}$$

where R_c is the local radius and β is the local angle of inclination of the conical cylinder. Another choice of boundary conditions on the undisturbed surface of the liquid at infinity is

$$y|_{x=\infty}=0 \tag{11}$$

$$\frac{dy}{dx}|_{x=\infty}=0 \tag{12}$$

Obviously, such boundary conditions cannot be implemented in practice.

By substituting $y_1=y$ and $y_2=dy/dx$ into Eq. (8), it can be transformed into

$$\frac{dy_1}{dx}=y_2 \tag{13}$$

$$\frac{dy_2}{dx}=\left[\frac{\Delta\rho g y_1}{\gamma_{lv}}-\frac{y_2}{x(1+y_2^2)^{1/2}}\right](1+y_2^2)^{3/2} \tag{14}$$

Consequently, the boundary conditions (Eqs. (9) and (10) or Eqs. (11) and (12) associated with Eq. (8) can be changed into the corresponding initial conditions:

$$y_1|_{x=R_c}=h \tag{15}$$

$$y_2|_{x=R_c}=\tan(\beta+\theta) \tag{16}$$

or

$$y_1|_{x=\infty}=0 \tag{17}$$

$$y_2|_{x=\infty}=0 \tag{18}$$

Eqs. (13) and (14) with the initial conditions Eqs. (15) and (16) form a set of first-order nonlinear ordinary differential equations for y_1 (i.e. y) and y_2 (i.e. dy/dx) as functions of the independent variable x. For given R_c, β, θ, h and $\Delta\rho g/\gamma_{lv}$, which depend on the shape of the conic cylinder and the properties of the liquid tested, the complete shape of the axisymmetric capillary rise profile $y=y(x)$ can be easily obtained by integrating the differential Eqs. (13) and (14) simultaneously with the initial conditions Eqs. (15) and (16). In this study, the four-order Runge–Kutta technique was used to solve the differential system. For the part of the liquid–vapour profile where $|dy/dx|$ is greater than 1.0, the differential system will be automatically switched to another set of first-order ordinary differential equations for x_1 (i.e. x) and x_2 (i.e. dx/dy). This can be done by using y as an independent variable and substituting

$$\frac{dy}{dx}=\frac{1}{\dfrac{dx}{dy}} \tag{19}$$

$$\frac{d^2y}{dx^2}=-\frac{1}{\left(\dfrac{dx}{dy}\right)^3}\frac{d^2x}{dy^2} \tag{20}$$

into Eq. (8). The detailed mathematical transformations of the differential equations as well as their initial conditions are straightforward, and are thus not included here. In this way it is ensured that the variation in the dependent variable in each step will definitely be less than the calculating step of the independent variable during the numerical calculation of the capillary rise profile, which can be chosen properly.

3. The objective function and its optimization

Like the ADSA technique [19–21], the ACRPAC method determines the contact angles from the shapes of the liquid–vapour interfaces, i.e. from the capillary rise profiles on a conical or constant-diameter cylinder. The strategy employed is to define an objective function which is a measure of the discrepancy between the physically observed capillary rise profile and the theoretically calculated curve, i.e. a curve satisfying the Laplace equation of capillarity. The objective function then is minimized numerically by using the contact angle as one of the adjustable parameters.

Let x_{mi} and y_{mi} ($i=1, 2, \ldots, N$) be a set of experimentally measured coordinates which describe the measured liquid–vapour interface, and x_{cj} and y_{cj} ($j=1, 2, \ldots, K$, choosing $x_{cK} > x_{mN}$) be another set of the coordinates of a calculated Laplacian curve. Here, the objective function E is defined as:

$$E = \frac{\sum_{i=1}^{N} |d_i|}{N} \tag{21}$$

where d_i is the "normal" distance from each measured point (x_{mi}, y_{mi}) to the calculated capillary rise profile ($i=1, 2, \ldots, N$). According to the above definition, physically the objective function is the average of the "normal" distances between the measured points and the theoretical Laplacian curve. Hence, the value of the objective function depends only on the shape of the calculated Laplacian curve once the real profile has been measured, i.e. x_{mi} and y_{mi} ($i=1, 2, \ldots, N$) are given.

In order to construct a theoretical Laplacian curve by solving Eqs. (13) and (14) with the initial conditions Eqs. (15) and (16), as described in the previous section, some necessary parameters (the local gravity g, the density difference between the liquid and the vapour phases $\Delta\rho$ and the liquid–vapour surface tension γ_{lv}) are assumed known. As will be discussed in the next section, for a given conical cylinder, Δh_m, R_c and β can be readily determined from the physically observed capillary rise profile, where Δh_m is the measured relative elevation of the position of the three-phase contact circle on the cylinder to the position of the lower edge of the acquired partial capillary rise profile. In the experiments, only the partial capillary rise profile could be acquired because of the contradiction between the image resolution and the scope of the microscope and video camera system. The calculated capillary rise profile around the conical cylinder in this study shows that the liquid–vapour interface can extend over quite a large range. It is practically impossible to acquire the complete capillary rise profile with sufficient image resolution. If h_0 represents the capillary rise height at the lower edge of the measured partial capillary rise profile relative to the undisturbed liquid surface, then the absolute height of the capillary rise h at the conical cylinder is equal to

$$h = h_0 + \Delta h_m \tag{22}$$

Therefore, once $\Delta\rho g/\gamma_{lv}$, Δh_m, R_c and β are known, the calculated Laplacian curve will depend only on the values of θ and h_0. Consequently, the objective function depends only on the two parameters θ and h_0:

$$E = E(\theta, h_0) \tag{23}$$

In the present optimization scheme, θ and h_0 are used as the adjustable parameters to find the best fit of the theoretical Laplacian curve to the digitized liquid–vapour interface. Once the objective function has been minimized, the corresponding value of θ is the measured contact angle. Thus for a given conical cylinder and a tested liquid, only a set of discrete coordinates of the physically observed capillary rise profile is required as input data. The output of the optimization scheme will provide the values of the contact angle θ and the capillary rise height h (or h_0), as well as the

calculated capillary rise profile corresponding to the minimum objective function E_{min}.

4. Digital image acquisition and digitization

A block diagram of the apparatus used in the present experiments is shown in Fig. 2. A coated glass cylinder is inserted into a shallow dish that has been slightly overfilled with the test liquid, and the set-up is placed between the light source and the microscope (Cohu 4910 CCD monochrome camera mounted on a Leica Wild M3B microscope). The video signal of the capillary rise profile is transmitted to a videopix digital video processor, which performs the frame grabbing and digitization of the image to 640×480 pixels with 256 grey levels each (zero represents black, 255 represents white). A SunSparc10 computer was used to acquire the image from the videopix and perform the image analysis, computation and digitization.

All experimental digital images were automatically stored in the computer memory. The basic aspects of the digital image acquisition process are as follows. A video source, such as a video camera attached to a microscope, produces an analogue video signal containing image data. This signal is transmitted to the image processor. The analogue signal is converted to a digital signal containing the image data in the form of digital picture elements, or pixels. The digital pixel data are then stored in frame memory one frame at a time, with each pixel occupying one frame memory location. Once the image has been stored in frame memory, it may be accessed for display or for additional computer processing. Display circuitry transforms the pixels stored in frame memory back into an analogue signal for display on a video monitor. The number of pixels transferred to or from frame memory in one frame time defines the display resolution of the frame memory.

Two typical images (produced by a laser printer) of the partial capillary rise profiles of the hexadecane–vapour (air) interface, one around the bottom-tip part and another around the conical part of a conical cylinder, are shown in Figs. 3(a) and 4(a), respectively. For each image, using a standard grid image as a calibration to correct possible optical distortion, a special computer image processing and analysis program was used to digitize the image automatically at subpixel resolution. The computer program then determines the profiles of the conical cylinder and the liquid–vapour interface. The output of this program is two sets of discrete coordinates, x and y (mm), of the profile of the cylinder surface and the capillary rise profile of the tested liquid on the left- and right-hand sides, respectively. The digitized plots (produced by a laser printer) of the images shown in Figs. 3(a) and 4(a) are given in Figs. 3(b) and 4(b), respectively. These plots clearly indicate the profiles of the cylinder surface and the hexadecane–vapour interfaces on both sides. By implementing the spline curve fitting, the accuracy of the digitized profiles is about 1.0 μm, at $\times 40$ magnification.

With the digitized profiles of each image, the local radius R_c of the three-phase contact circle is half the horizontal difference between the three-phase contact points on the left side and on the right side. The relative elevation between the three-phase contact circle and the lower edge of the partial capillary rise profile covered by the image Δh_m, as defined previously, is merely their vertical difference. The local slope of the solid surface profile, i.e. $\tan \beta$, at the position of the three-phase

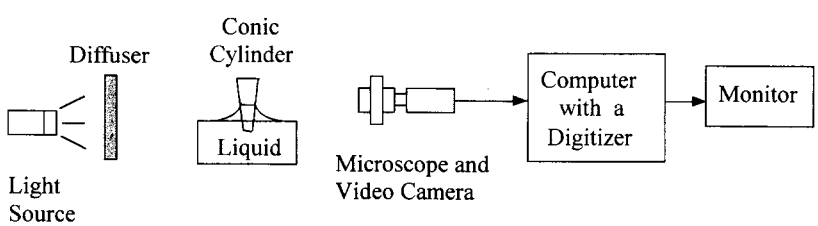

Fig. 2. Experimental set-up used to measure the contact angle by analysis of the capillary rise profile around a cylinder (ACRPAC).

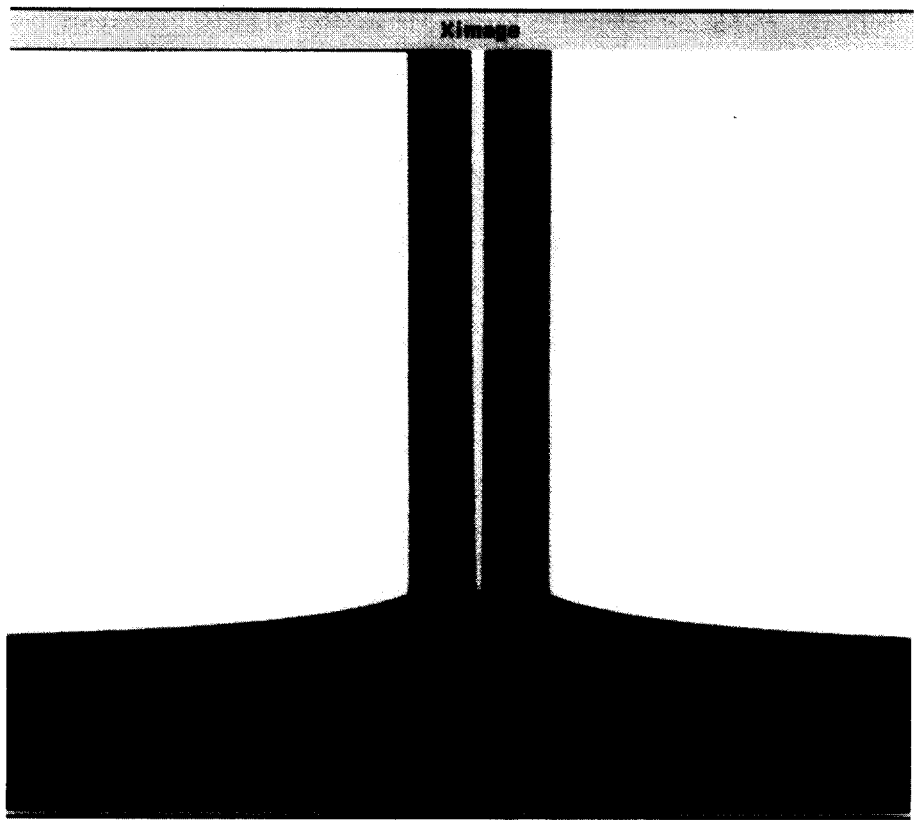

(a)

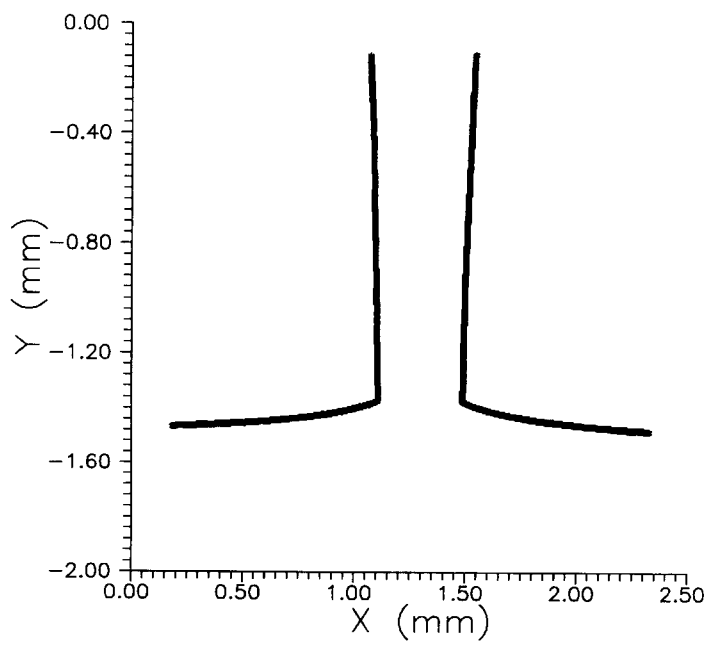

(b)

Fig. 3. (a) Digital image of the capillary rise profile of hexadecane around an FC725 coated conical cylinder at its tip. (b) Digitization of the image shown in (a). Both images were reproduced on a laser printer.

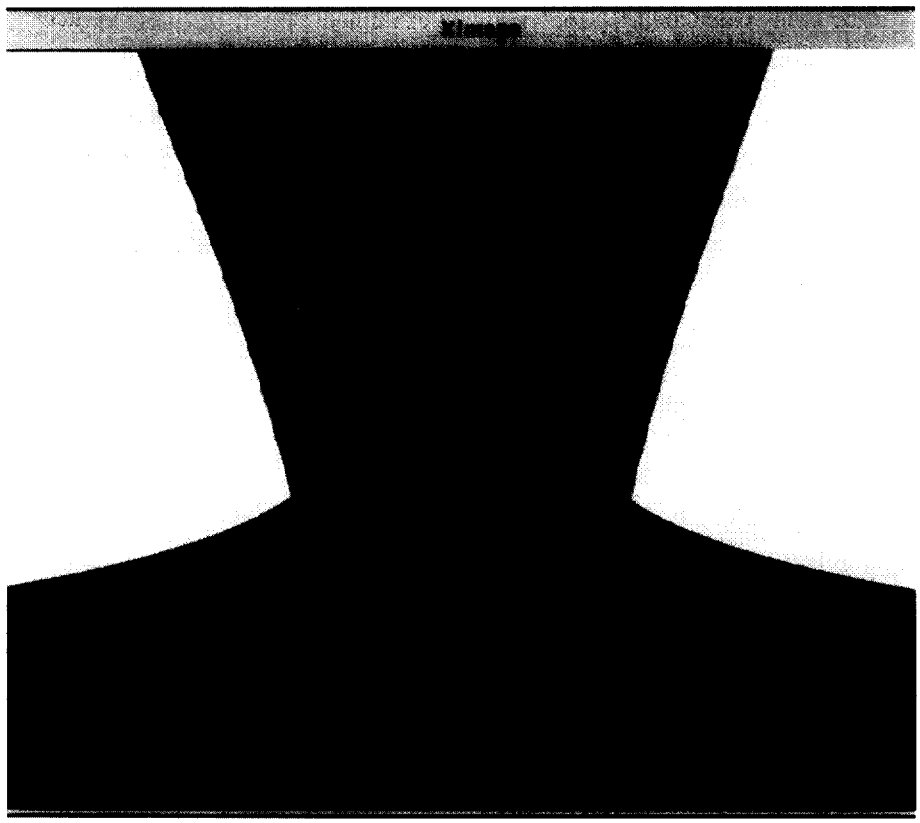

(a)

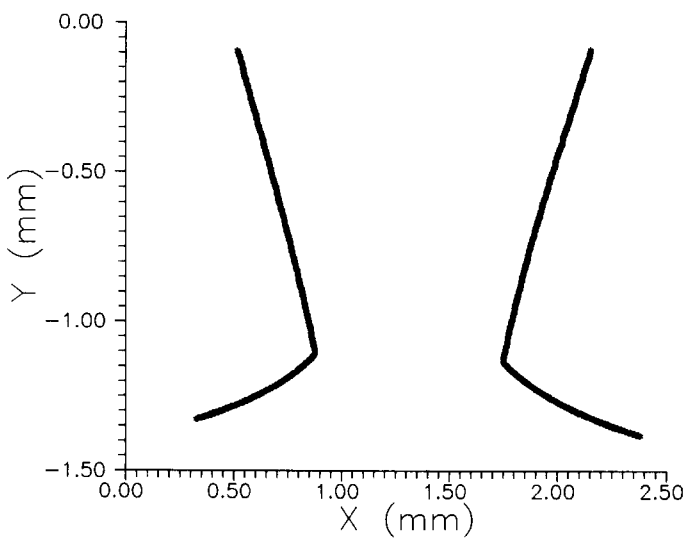

(b)

Fig. 4. (a) Digital image of the capillary rise profile of hexadecane around an FC725 coated conical cylinder on its conical part. (b) Digitization of the image shown in (a). Both images were reproduced on a laser printer.

contact circle can be easily calculated by applying a polynomial fitting program to the measured profile of the solid surface.

5. Experimental

The liquids used in the present contact angle measurements were decane, dodecane, tetradecane and hexadecane (Aldrich, 99% pure). These liquids were chosen in order to satisfy the following general requirements: they have low vapour pressure or a high boiling temperature so as to minimize adsorption; they are chemically stable and not excessively toxic; and they will form finite contact angles at the solid surface used in this study. In addition, the contact angles θ_∞ and line tensions σ of these liquids on a similar solid surface, FC721, are available in the literature [9,10,12].

In the present work, the solid surface used in the experiments was a fluorochemical surfactant coating material, FC725 (3M Product), coated on very smooth glass cylinders. Two types of glass cylinder were used: constant-diameter cylinders and conical (varying diameter) cylinders. As illustrated in Fig. 1, the local radius R_c of the conical cylinder changes smoothly from approximately 0.14 mm at the tip to 1.0 mm (or 1.5, 2.5 mm) at its upper cylindrical part. The local inclination angle β, defined as the angle between the gradient of the cylinder profile and the horizontal level, decreases from 90° near the tip, reaches a minimum of about 60° at the conical part, and finally increases to 90° again at the upper cylindrical part. The FC725 surface was prepared by a dip-coating method as described below. First, the cylinder was slowly and vertically dipped into a small bottle filled with FC725. The bottle was placed on a disk floating on the surface of water in a beaker. The position of the floating disk, and hence the level of the coating liquid, were then lowered very slowly by draining the water in the beaker at a controlled rate. Thus, a uniform and smooth coating of FC725 was left on the cylinder. Finally, the coated cylinder was suspended vertically and dried in air before use in the experiment.

The quality of the FC725 surfaces was carefully examined. First, it was known from the 3M Product Selection Guide that this fluorochemical surfactant coating material is very stable, even in many extremely aggressive chemical environments. The FC725 coating material is insoluble in organic liquids such as the n-alkanes used in this study. Secondly, the average roughness of the dip-coated FC725 surfaces, measured by using a Tencor Surface Profilometer (TSP), was less than 0.0250 μm. Finally, the contact angle hysteresis was measured by using the following procedures. To avoid line tension effects, contact angle measurements were done on the FC725 coated glass cylinders of constant radius (i.e. $\beta = 90°$). Initially, the coated cylinder was slowly inserted vertically into the test liquid to a certain depth. Thirty seconds was given to allow the three-phase contact line and the liquid meniscus to reach equilibrium. An image of the capillary rise profile around the cylinder was then taken. The cylinder was inserted further into the liquid so that the three-phase line reached a new position, and a new image was taken after 30 s, and so on until five advancing contact angles had been measured from successive digital images, each at a different vertical position along the cylinder. Afterwards, five receding contact angles were measured in a similar way by moving the cylinder upwards. For a given liquid, the above measurements were repeated for three separate cylinders. For all liquids tested in this work, the contact angle hysteresis is almost same (5–7°). For example, for the FC725-tetradecane system, the average advancing contact angle is 65.3° and the average receding contact angle is 58.4°. Although the solid surfaces used in this work were very smooth, they may still have had a very small percentage of heterogeneity, probably due to impurities of the coating material and dust in the air. This might be the cause of the observed contact angle hysteresis. It has been shown [32] that the advancing contact angle on a smooth but heterogeneous surface represents the equilibrium properties of the dominant material of the surface, while the receding contact angle reflects the properties of the impurity of the surface. Hence, the contact angles mentioned hereafter will be the advancing contact angles.

Measurements of the capillary rise profile

around a conical cylinder were carried out according to the following procedure. For each liquid, three conical cylinders of different sizes were used in the measurement. First, the tip part of the conical cylinder was inserted in the liquid and the image of the capillary rise profile around that part was taken. Then the conical cylinder was moved down very gently to change the position of the three-phase contact circle on the cylinder. Once the capillary rise profile around the cylinder had formed and become stable, another image was taken at the new position, and the experiment continued until the profile reached the upper cylindrical part. Contact angle measurements for constant-diameter cylinders were accomplished in a similar fashion. The entire experimental set-up was placed on a vibration-free table. All measurements were conducted at 22°C.

For comparison, the ADSA and the Wilhelmy plate techniques were also used to measure the contact angles of the same solid–liquid systems. The glass slides (7.5 cm × 2.5 cm) used in the measurements were coated with FC725 by the same dip-coating method as described above. In the first experiment the contact angle of a sessile drop on a FC725-coated glass slide was measured by applying the ADSA technique. This technique has been used extensively and described in detail elsewhere [19–21]. Secondly, the Wilhelmy plate technique was employed to determine the contact angle with no line tension effect θ_∞ at the vertical slide. Once the capillary rise height h had been measured, the contact angle was calculated from Eq. (1). The measurement procedures used in the present study can be summarized as follows. A vertical glass slide coated with FC725 was dipped into a shallow dish that had been slightly overfilled with the test liquid. The slide was then placed between a light source and a goniometer. The dish was wide enough to ensure that the liquid surface was horizontal in the region far from the glass slide. A goniometer was installed on a three-dimensional translation stage with a vertical resolution of 1.0 μm. The stage was mounted on a separate stand to insulate any mechanical vibrations created by its movement. Using the goniometer and the translation stage, the height of capillary rise was determined by measuring the position of the three-phase contact line on the coated glass slide and the position of the horizontal liquid surface. For an individual measurement of h, a total of ten readings of the position of the horizontal liquid surface and the position of the three-phase contact line were taken.

6. Results and discussion

6.1. Contact angle measurements on constant-diameter cylinders

Experiments were conducted to test the ACRPAC method. As a first application, the contact angles on FC725-coated constant-diameter cylinders for the four n-alkane liquids (decane, dodecane, tetradecane and hexadecane) were measured. To examine the possible effect of cylinder size on the measured contact angles, three cylinders of different sizes ($R_c = 1.0$, 1.5 and 2.5 mm) were used for each liquid. Ten images were taken at different positions of each cylinder. The consistency of the measured contact angles between the three different sized cylinders indicates that the cylinder size had no appreciable effect on the results. Physically, these measured contact angles are the advancing contact angles with no line tension effect $\theta_{\infty ACRPAC}$, since the constant-diameter cylinders were positioned vertically, i.e. $\beta = 90°$, as explained in the next section (see Eq. (27). According to the classical Young equation, these contact angles only depend on the interfacial tensions of the solid–liquid–vapour interfaces in the system.

Table 1 shows the average contact angle value

Table 1
Contact angles for four n-alkane liquids on FC725-coated constant-diameter cylinders, as measured with the ACRPAC technique and the Wilhelmy plate technique

Solid–liquid system	γ_{lv} (mJ m^{-2})	$\theta_{\infty ACRPAC}$ (°)	$\theta_{\infty Wilhelmy}$ (°)
FC725–decane	23.43	58.7 ± 0.38	58.9 ± 0.49
FC725–dodecane	25.44	63.7 ± 0.37	63.3 ± 0.51
FC725–tetradecane	26.55	65.8 ± 0.48	65.4 ± 0.50
FC725–hexadecane	27.76	69.8 ± 0.41	69.2 ± 0.46

(at the 95% confidence interval) of each liquid measured with the ACRPAC method. For comparison, the contact angles $\theta_{\infty \text{Wilhelmy}}$ (at the 95% confidence interval) of each liquid obtained with the Wilhelmy plate technique are also given. The agreement between the results obtained with these two techniques is very good. However, it is noted that the measured contact angles have a maximum variation of about $\pm 0.5°$ around the mean values. This is due to the practical difficulty in aligning either the cylinder or the slide truly vertically in the measurements. The results indicate that a slight inclination of the cylinder or the slide could cause a rather large difference in the measured contact angles between the left and the right sides. The 95% confidence interval is only about $\pm 0.1°$ if the measured contact angles from only one side are averaged. Therefore, the accuracy of the contact angles measured with the ACRPAC technique is approximately 0.1°.

6.2. Contact angle measurements on conic cylinders

The contact angles on the FC725-coated conical cylinders for the four n-alkane liquids were also measured using the ACRPAC technique. As an example, Table 2 shows the changing contact angles of decane at the FC725 solid surface at different positions on a conical cylinder, from its lower tip to its upper cylindrical part. The contact angles at the conical part are approximately 3–4° larger than those at the cylindrical part. This phenomenon can be interpreted in terms of the so-called line tension effect. Hence, a direct application of the present experimental technique is to determine line tension by measuring the contact angles at different positions on a conical cylinder.

Table 2
Variation in the contact angle (θ) of decane at a FC725-coated conical cylinder along its axial direction, with the local values of the radius (R_c) and the inclination angle (β) at the three-phase contact circle

Image no.	R_c (mm)	β (°)	θ (°)
1	0.1937	86.7	59.5
2	0.1997	85.1	62.4
3	0.2363	82.6	62.5
4	0.2607	82.2	62.0
5	0.3539	70.3	63.2
6	0.4240	68.5	62.3
7	0.4378	67.4	63.6
8	0.8614	70.4	60.0
9	1.0234	88.5	59.3
10	1.0313	88.7	59.0

A detailed discussion of the line tension effect and its determination from contact angles measured around a conic cylinder has been given previously [22]. In surface thermodynamics, the line tension in a three-phase equilibrium system can be defined as either the free energy per unit length of a three-phase contact line [33,34] or the force operating in a one-dimensional three-phase contact line and tending to minimize its length. For a sessile drop on an ideal solid surface, the mechanical equilibrium condition at any point along the three-phase contact circle can be expressed by the modified Young equation [34]:

$$\cos\theta = \cos\theta_\infty - \frac{\sigma}{\gamma_{lv}}\frac{1}{R} \tag{24}$$

and

$$\cos\theta_\infty = \frac{\gamma_{sv} - \gamma_{sl}}{\gamma_{lv}} \tag{25}$$

where γ_{lv}, γ_{sv} and γ_{sl} are the interfacial tensions of the liquid–vapour interface, the solid–vapour interface and the solid–liquid interface, respectively; R is the radius of the three-phase contact circle; θ is the advancing contact angle corresponding to a finite contact radius R; θ_∞ is the contact angle corresponding to an infinitely large drop, i.e. $R = \infty$; and σ is the line tension. The well-known classical Young equation (Eq. (25) indicates that θ_∞ is constant for a given solid–liquid–vapour system. The modified Young equation (Eq. (24) relates the line tension to the contact angle and the radius of a three-phase contact circle. Thus, the line tension can be determined by measuring the dependence of the contact angle on the drop size. As defined in Eq. (24), the slope of the $\cos\theta$ vs. $1/R$ straight line is $(-\sigma/\gamma_{lv})$. If the slope and the liquid surface tension are known, the line tension can be determined.

Recently, Lin and Li [35] have incorporated the local inclination angle β of an inclined solid sur-

face, or a solid surface of revolution in the form of cos β, into the line tension term in Eq. (24). They derived another form of the modified Young equation for the case where the three-phase line is in contact with an inclined solid surface:

$$\cos\theta = \cos\theta_\infty - \frac{\sigma}{\gamma_{lv}}\frac{\cos\beta}{\rho} \quad (26)$$

where ρ is the local radius of curvature of the three-phase contact line. Eq. (26) clearly shows the influence of the local inclination angle β on the curvature ($1/\rho$) dependence of the contact angles due to the line tension effect. For an ideal solid surface of revolution, such as a cone or cylinder, the three-phase contact line is a circle because of its axisymmetry and ρ becomes a constant R_c, the local radius of the contact circle on the solid surface. Therefore, Eq. (26) can be simplified as

$$\cos\theta = \cos\theta_\infty - \frac{\sigma}{\gamma_{lv}}\frac{\cos\beta}{R_c} \quad (27)$$

Eq. (27) will reduce to Eq. (24) if $\beta = 0°$, i.e. if cos $\beta = 1$, which corresponds to a horizontal planar solid surface. It then becomes the classical Young equation (Eq. (25) if $\beta = 90°$ (i.e. cos $\beta = 0$) and $\theta = \theta_\infty$, which corresponds to either a vertical cylinder with a constant radius, as discussed in the previous section, or a vertical flat plate as used in the Wilhelmy plate technique [1,15,23,24]. In such a case, the line tension term is absent from Eq. (27). Therefore, θ_∞ should be defined more exactly as the contact angle with no line tension effect. However, the linear relationship between cos θ and (cos β/R_c) for a given solid–liquid system predicted by Eq. (27) has yet to be confirmed experimentally.

It should be noted that the advancing contact angle measured on a real surface is the Young contact angle, i.e. the angle that can be used in the Young equation [36]. Since the conditions required to derive Eq. (27) are the same as those required to derive the classical Young equation, the advancing contact angles can also be used in Eq. (27). It has also been shown elsewhere [32,36] that the advancing contact angle represents the equilibrium property of the dominant material of a smooth but non-homogeneous surface. Thus, the line tensions calculated from the advancing contact angles represent the property of the dominant material, the FC725 in the present case. Nevertheless, since the solid surfaces used in this study show some contact angle hysteresis, albeit small, interpretation of the contact angle data by using Eq. (27) may not give the true line tensions. Therefore, the line tension values reported in this study may be referred to the "pseudo-line tension" values [7].

By employing the present experimental technique, the quantities in Eq. (27), such as the radius of the three-phase contact circle R_c, the inclination angle β and the contact angle θ, can be measured directly as described in the previous sections. Therefore, the remaining tasks are to bring the measured R_c, β and θ into the modified Young equation (Eq. (27) and then plot the data in terms of cos θ vs. cos β/R_c. The line tension σ and the contact angle θ_∞ can be readily calculated, since the gradient and the intercept of the fitted linear line to these data are $-\sigma/\gamma_{lv}$ and $\cos\theta_\infty$, respectively.

The experimental data obtained in this work and the corresponding linear lines fitted using Eq. (27) for the four liquids on the FC725 surface are shown in Fig. 5. The correlation coefficients

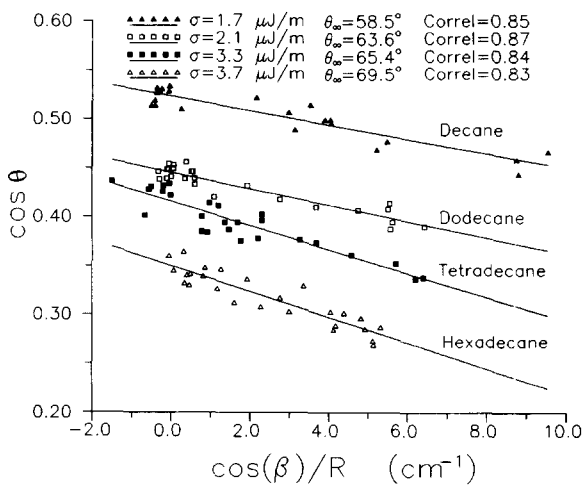

Fig. 5. The line tensions (σ) and contact angles (θ_∞) derived from Eq. (27) using the contact angles measured using the ACRPAC technique for the four n-alkane liquids on the FC725-coated conical cylinders.

for these fitted linear functions are all above 0.83. Therefore, the linear relationship between cos θ and cos β/R_c as predicted by Eq. (27) is statistically supported by these data. The line tension σ and the contact angles θ_∞ for the four *n*-alkanes on the FC725 surface were obtained from the plots in Fig. 5, and summarized in Table 3. These line tension values agree well with those reported in the literature for similar systems [8–10]. In order to examine the validity of the contact angles θ_∞ and line tensions σ derived from the measured contact angles around a conical cylinder, comparative experiments were done. For each liquid on the FC725-coated glass slides, the contact angles θ_{ADSA} of sessile drops with a contact radius R of 3 mm were measured using the ADSA technique. The results are listed in the last column of Table 3. In addition, the contact angles were calculated using Eq. (24) with $R=3$ mm and the derived θ_∞ and σ values listed in Table 3. These predicted contact angles θ_{pred}, are also listed in the table. For all four liquids, these two contact angles are in excellent agreement, within the experimental error.

As discussed before, in the sessile drop method the contact angle without line tension effect θ_∞, corresponds to the contact angle of an infinitely large drop. In the sessile drop method, θ_∞ can only be evaluated [8–10] by extrapolating the fitted line of cos θ versus $1/R$ to the vertical axis (i.e. $1/R=0$), because in practice it is impossible to generate an infinitely large drop. For the conical cylinder–liquid systems, however, both the local radius R_c of the three-phase contact circle and the local inclination angle β of the solid surface can be changed simultaneously. The quantity cos β/R_c in Eq. (27) covers a wider range, in this study approximately -1.00 to $10.00\ cm^{-1}$. More importantly, the point cos $\beta/R_c=0$ is also included in this range. At this point, cos θ becomes cos θ_∞ and the line tension effect is removed from Eq. (27). Hence, the contact angle without line tension effect θ_∞, which is derived from the contact angles measured by the ACRPAC technique, is more reliable. In fact, this conclusion is also supported by the excellent consistency between the θ_∞ values derived from Eq. (27) (Table 3) and those measured directly either by the ACRPAC method or the Wilhelmy plate technique (Table 1).

7. Summary

A new contact angle measurement technique by analysis of capillary rise profile around a cylinder (ACRPAC) has been presented. In this method, computer image processing and analysis techniques are used to obtain the profiles of the cylinder and the liquid–vapour interface around the cylinder. The contact angle is determined by numerically minimizing the discrepancy between the physically observed liquid–vapour interface and the theoretically predicted capillary rise profile, i.e. the curve representing a solution of the Laplace equation of capillarity. The input requirements are the density difference between the liquid and the vapour phases, the liquid–vapour surface tension and the local gravity. The present technique was successful in measuring the contact angles of capillary rise profiles around a constant-diameter or conical

Table 3
The line tensions (σ) and the contact angles (θ_∞) for four *n*-alkane liquids on the FC725-coated solid surface, as derived from Eq. (27) by using the contact angles measured on a conical cylinder

Solid–liquid system	γ_{lv} (mJ m^{-2})	σ (μJ m^{-1})	Correl.[a]	θ_∞ (°)	θ_{pred} ($R=3$ mm) (°)	θ_{ADSA} ($R\approx3$ mm) (°)
FC725–decane	23.43	1.7	0.85	58.5	60.2	59.9
FC725–dodecane	25.44	2.1	0.87	63.6	65.8	66.3
FC725–tetradecane	26.55	3.3	0.84	65.4	68.0	68.2
FC725–hexadecane	27.76	3.7	0.83	69.5	71.4	71.2

[a] The correlation coefficient of the linear fitting.

cylinder. The measured contact angles agree very well with those measured using the Wilhelmy plate technique or the ADSA technique for the sessile drop case, respectively. The present technique is a powerful alternative tool for accurate measurements of contact angles on fibres. It will be particularly useful in studies of the wetting, spreading and adhesion processes of a liquid on fibre surfaces. A general user-oriented computer program package for implementing this technique is available.

Acknowledgment

This study was supported by the Natural Sciences and Engineering Research Council of Canada (Grant No. OPG0155248). The authors also thank Dr. Ken Westra, Alberta Microelectronic Centre (AMC), for his technical assistance in measuring the roughness of the coated solid surfaces.

References

[1] A.W. Adamson, Physical Chemistry of Surfaces, 4th edn, Wiley, New York, 1982.
[2] A.W. Neumann, D.R. Absolom, W. Zingg, C.J. van Oss and D.W. Francis, in Biocompatible Polymers, Metals and Composites, M. Szycher (Ed.), 1983, p. 53.
[3] A.W. Neumann, D.R. Absolom, D.W. Francis, S.N. Omenyi, J.K. Spelt, Z. Policova, C. Thomson, W. Zingg and C.J. van Oss, J. Ann. NY Acad. Sci., 416 (1983) 276.
[4] D. Li and A.W. Neumann, Adv. Colloid Interface Sci. 39 (1992) 299.
[5] A. Marmur, J. Colloid Interface Sci., 148 (1992) 541.
[6] B.V. Toshev and D. Platikanov, Adv. Colloid Interface Sci., 40 (1992) 157.
[7] R.J. Good and M.N. Koo, J. Colloid Interface Sci., 71 (1979) 283.
[8] J. Gaydos and A.W. Neumann, J. Colloid Interface Sci., 120 (1987) 76.
[9] D. Li and A.W. Neumann, Colloids Surfaces, 43 (1990) 195.
[10] D. Duncan, D. Li, J. Gaydos and A.W. Neumann, J. Colloid Interface Sci., 169 (1995) 256.
[11] J.A. Wallace and S. Schürch, Colloids Surfaces, 43 (1990) 207.
[12] M. Yekta-Fard and A.B. Ponter, J. Colloid Interface Sci., 126 (1988) 134.
[13] J.F. Padday, in Surface and Colloid Surface, E. Matijevic (Ed.), Vol. 1, Wiley, New York, 1968, pp. 101–149.
[14] D.S. Ambwani and T. Fort, Jr., in Surface and Colloid Science, R.J. Good and R.R. Stromberg (Eds), Vol. 11, Plenum, New York, 1979, pp. 93–119.
[15] A.W. Neumann and R.J. Good, in Surface and Colloid Science, R.J. Good and R.R. Stromberg (Eds), Vol. 11, Plenum, New York, 1979, pp. 31–91.
[16] S. Wu, Polymer Interface and Adhesion, Marcel Dekker, New York, 1982.
[17] L.M. Lander, L.M. Siewierski, W.J. Brittain and E.A. Vogler, Langmuir, 9 (1993) 2237.
[18] J.E. Seebergh and J.C. Berg, Chem. Eng. Sci., 47 (1992) 4468.
[19] Y. Rotenberg, L. Boruvka and A.W. Neumann, J. Colloid Interface Sci., 93 (1983) 169.
[20] P. Cheng, D. Li, L. Boruvka, Y. Rotenberg and A.W. Neumann, Colloids Surfaces, 43 (1990) 151.
[21] D. Li, P. Cheng and A.W. Neumann, Adv. Colloid Interface Sci., 39 (1992) 347.
[22] Yongan Gu, Dongqing Li and P. Cheng, J. Colloid Interface Sci., 180 (1996) 212.
[23] A.W. Neumann, Adv. Colloid Interface Sci., 4 (1974) 105.
[24] C.J. Budziak and A.W. Neumann, Colloids Surfaces, 43 (1990) 279.
[25] J. Yamaki and Y. Katayama, J. Appl. Polym. Sci., 19 (1975) 2897.
[26] B.J. Carroll, J. Colloid Interface Sci., 57 (1976) 488.
[27] H.D. Wagner, J. Appl. Phys., 67 (1990) 1352.
[28] M. Nardin and I.M. Wards, Mater. Sci. Technol., 3 (1987) 814.
[29] T. Ogawa and M. Ikeda, J. Adhesion, 43 (1993) 69.
[30] A. Kumar and S. Hartland, J. Colloid Interface Sci., 124 (1988) 67.
[31] A. Kumar and S. Hartland, J. Colloid Interface Sci., 136 (1990) 455.
[32] D. Li and A.W. Neumann, Colloid Polym. Sci., 270 (1992) 498.
[33] J.W. Gibbs, The Scientific Papers, Vol. 1, Dover, New York, 1961, p. 288.
[34] L. Boruvka and A.W. Neumann, J. Chem. Phys., 66 (1977) 5464.
[35] F.Y.H. Lin and D. Li, Colloids Surfaces, 87 (1994) 93.
[36] A.W. Neumann and R.J. Good, J. Colloid Interface Sci., 38 (1972) 341.